Novel transmitter designs for magnetic resonance imaging
Aussenhofer, S.A.

Citation
Aussenhofer, S. A. (2018, April 11). *Novel transmitter designs for magnetic resonance imaging*. Retrieved from https://hdl.handle.net/1887/61005

Cover Page

Universiteit Leiden

The following handle holds various files of this Leiden University dissertation:
http://hdl.handle.net/1887/61005

Author: Aussenhofer, S.A.
Title: Novel transmitter designs for magnetic resonance imaging
Issue Date: 2018-04-11

3

HIGH-PERMITTIVITY SOLID CERAMIC RESONATORS FOR HIGH-FIELD HUMAN MRI

Sebastian A. AUSSENHOFER

Andrew G. WEBB

3

The properties of a ceramic-based annular dielectric resonator designed for 7 T MRI have been examined. Electromagnetic simulations and experimentally determined modal frequencies agree to within 1%. The dependence of the resonance frequency of the degenerate quadrature HEM_{11} modes on hole diameter and shield diameter was also investigated. The constructed coil, with a 2.5 cm diameter hole, had an unloaded Q value of 400, which was reduced to 150 when loaded with a human finger. Simulated and experimental B_1^+ maps show a high degree of homogeneity with a sensitivity of $\sim 11.5\,\mu T/\sqrt{W}$ at the centre. A comparison with a loop gap resonator showed an approximately 25% higher sensitivity for the dielectric resonator. High-resolution images of the digital interphalangeal (DIP) and proximal interphalangeal (PIP) joints of volunteers were acquired in imaging times of less than 2 min. Finally, novel methods of double tuning such ceramic resonators to two relatively close frequencies, e.g. proton and fluorine, have been shown.

3.1. INTRODUCTION

THE majority of RF coils for MRI are constructed from electrically conductive elements, usually consisting of copper or silver-coated copper. A potential alternative is to use high-permittivity, low-loss ceramic materials (either as the coil itself or as an insert), as has been shown in a few resonator designs for electron paramagnetic resonance [2], [3] and MR imaging and spectroscopy [4], [5], [6], [7], [8], [9] and [10]. Several different spatially variant electromagnetic modes of magnetic field storage exist for different geometries of the high-permittivity material. The most common geometry is an annulus into which the sample is placed, although arrangements of two disks with a small gap between have also been demonstrated [5]. For the majority of these resonators, the transverse electric (TE_{01}) mode has been used. This is the lowest-frequency mode, but for MR applications has the disadvantage that it is only a linear mode (thus cannot be driven in quadrature), and that the B_1 field lies along the axial dimension of the cylinder, thus making it somewhat disadvantageous for realistic in vivo applications as the coil has to be rotated through $90°$ perpendicular to the B_0 field [10]. The first practical RF resonator operating in a circularly polarized degenerate hybrid electromagnetic mode (HEM_{11}) was designed with water as the high-permittivity material, and was used to image the human wrist on a 7 T whole-body scanner [11]. One of the major advantages of the resonator was its very easy construction from readily available materials. However, water is a relatively lossy dielectric even at radio frequencies, gives a large background signal (although it can easily be replaced by deuterium oxide), and the relative permittivity of only 80 means that resonators can become quite large.

In this paper the properties and design of a solid, high-permittivity, low-loss ceramic HEM_{11}-mode resonator are described. The resonator is an annular design constructed from barium strontium titanate (BST). This material is based on the most most common high-permittivity material, barium titanate, which is doped with strontium. Doping reduces the Curie temperature (TC) of BST compared with barium titanate, with the result that BST has significantly lower loss than barium titanate, but also a lower relative permittivity (11). The exact value of the permittivity is highly dependent on grain size, generally increasing with decreasing grain size up to the sub-micron range. Commercially available barium titanate has a real component of the permittivity ~1400 with loss tangents ~0.05. Typical values for BST are 150–200 and 0.01, respectively.

The dimensions of the resonator are designed so that high- resolution imaging of human digits (for studies of rheumatoid arthritis) can be acquired with the resonator

having appropriate dimensions for a high filling factor and patient comfort. Extensive resonator characterization is performed, with experimental and simulation results compared. High-resolution in vivo images are acquired showing fine detail, in particular, of the cartilage structure in the finger. Finally, it is shown that one can take advantage of the independence of the single TE and two HEM modes to produce double-tuned probe designs for nuclei such as protons and fluorine whose gyromagnetic ratios are similar.

3

3.2. EXPERIMENT

3.2.1. HIGH-PERMITTIVITY CERAMIC MATERIALS

BARIUM strontium titanate cylinders with a relative permittivity ~175 (product K-175) and loss tangent less than 0.01 were purchased from TCI Ceramics/National Magnetics Group. The HEM$_{11}$ mode frequency is given by [12]

$$f_{HEM_{11\delta}} = 2.735 \frac{c\epsilon_r^{-0.436}}{2\pi a} \left[0.543 + 0.589\frac{a}{h} - 0.05\left(\frac{a}{h}\right)^2 \right] \tag{3.1}$$

where c is the speed of light, ϵ_r the relative permittivity, a the radius and h the height of the resonator. Since a hole has to be drilled in the cylinder and a shield placed around the ceramic to reduce radiation losses, and both of these increase the resonant frequency, the diameter was chosen to be less than would be predicted from Equation 3.1. Given that the coil was intended to image the finger, a height of at least 6 cm was required, and an inner annular diameter of at least 2.5 cm. Electromagnetic simulations (see below) were used to determine the final height and diameter of the ceramic disk as 6.3 cm and 8.6 cm, respectively, with a 2.5 cm hole in the centre. Ultrasonic-mediated milling was used to produce the central hole in the resonator.

3.2.2. ELETROMAGNETIC SIMULATIONS

Electromagnetic (EM) simulations of the magnetic field distributions for both the cylindrical (i.e. before drilling) and annular HEM resonators were performed using an eigenmode solver (CST Microwave Studio, Darmstadt, Germany). A tetrahedral mesh with 58 264 elements was created using the Delaunay meshing algorithm, with the maximum curved element order of six. Twenty modes were searched for above a frequency of 200 MHz, with an accuracy of 1×10^6, and a second-order convergence criterion. Two-dimensional vector plots were obtained to identify the particular mode based on known distributions of magnetic and electric fields [13]. The magnetic and electric fields are in quadrature, with the maximum values of the electric fields occurring at a phase of 0° and magnetic fields at 90°.

3.2.3. ELECTRICAL CHARACTERIZATION

Modal frequencies were measured using an unmatched, 1 cm diameter shielded loop constructed from semi-rigid 50 Ω coaxial cable (Microstock, West Point, PA). The loop was placed above the centre of the ceramic disc to detect primarily TE modes, and at the side of the resonator at half-height to detect HEM modes. For the HEM resonator standard inductive coupling loops [11] were used for impedance matching, with variable

capacitors for fine adjustment for different loads. For the impedance-matched resonator S_{11} measurements were performed for each quadrature channel, and an S_{12} measurement to determine the orthogonality of the modes. In order to characterize the loading effects on the coil, a saline phantom made of a plastic tube of 24 mm outer diameter and a length of 120 mm, with salt added to give a conductivity of 0.47 S/m, was used. This phantom was also used to produce B_1^+ maps.

3.2.4. MRI EXPERIMENTS

All imaging and B_1^+ mapping experiments were conducted on a 7 T whole-body human MRI scanner (Philips Achieva, Best, The Netherlands) using a dual TR method [14]. A three-dimensional gradient echo sequence was used with the following parameters: field of view $160 \times 160 \times 160$ mm^3, voxel resolution $2.5 \times 2.5 \times 2.5$ mm^3, TR_1/TR_2 30/150 ms, TE 1.5 ms, nominal 45° tip angle at the centre of the phantom. The coil sensitivity was calculated as the B_1^+ per square root watt of input power, with the power estimated from the output power of the RF amplifier taking into account measured power loss in the cables from the amplifier to the coil.

For imaging the finger, after acquiring short scout scans to determine the appropriate field of view, a three-dimensional gradient echo sequence was acquired with the following parameters: TR/TE 10 ms/5 ms, tip angle 10°, field of view $50 \times 100 \times 25$ mm^3, data acquisition matrix $332 \times 340 \times 50$ (zero-filled to $800 \times 800 \times 50$ for image display), spatial resolution $0.15 \times 0.3 \times 0.5$ mm^3, total image acquisition time 86 s. The study adhered to the LUMC Institutional Review Boardguidelines and informed consent was obtained from volunteers prior to the study.

3.2.5. REFERENCE RESONATOR

In order to compare the performance of the dielectric resonator design with a conventional design, a loop gap resonator [15] was built. An inner diameter of 2.5 cm was chosen to allow imaging the same phantom as for the ceramic resonator. The length was ~6 cm, and the loop was constructed from 25 μm thick copper foil (3M, St. Paul, Minnesota) shaped around a custom-produced plastic cylinder with a thickness of 1 mm. A conventional capacitive pi-network was used for impedance matching.

3.3. RESULTS

3.3.1. ELECTROMAGNETIC SIMULATIONS AND ELECTRICAL CHARACTERIZA-TION

T HE properties of the resonator were investigated using a simple unmatched 1 cm diameter shielded pick-up loop. Figure 3.1 shows network analyser plots for the solid resonator, annular resonator with no load, and annular resonator with a tissue-mimicking load. Table **??** shows a comparison between the simulated and measured frequencies of the first five modes. Based upon the mode behaviour with respect to the pick-up loop geometry and position, known modal patterns of the magnetic field distribution [13] and previous MRI-confirmed modal assignations [16], the modes can easily be assigned. The degenerate HEM mode has a well characterized magnetic and electric field distribution [11],[13], with a maximum in the magnetic field and zero electric field at the centre of the resonator. In general, a displacement of the electric and magnetic fields affects the resonant frequency, and its direction of change can be determined from cavity perturbation theory [17],[18].

$$\frac{\omega - \omega_0}{\omega_0} \approx \frac{\int\int\int_{\triangle v} \left(\mu|H_0^2| - \epsilon|E_0^2|\right) \partial v}{\int\int\int_v \left(\mu|H_0^2| + \epsilon|E_0^2|\right) \partial v} \tag{3.2}$$

where the numerator represents the difference of stored magnetic and electric energy within the volume $\triangle v$ and the denominator is the total energy stored within the volume v. Since ϵ is much larger than μ, the dominant factor is the displacement of the electric field. Drilling a hole in the centre of the resonator will have the smallest effect on the frequency of the TE_{011} mode and the largest effect on the TM_{011} mode, as shown in Table 3.1, since the TE mode has zero electric field, whereas the TM mode has its maximum electric field, along the central axis of the cylinder. In terms of an outer shield, if the stored energy outside the resonator is mostly electric, moving a metal shielding wall closer to the resonator will decrease the resonant frequency. Conversely, for a displaced field that is predominantly magnetic, the resonant frequency will increase. The small increases in frequency of the two TE and two HEM modes shows that a fraction of the magnetic energy is indeed stored outside the resonator.

Mode	Solid simu- lated	Solid experi- ment	Annular (2.5 cm hole) simulated	Annular (2.5 cm hole) experiment	Annular + shield simulated	Annular + shield experiment
TE_{011}	251.1	251.4	253.3	251.5	269.4	272.2
HEM_{11}	271.3	271.4	296.3	292.5	301.6	301.1
HEM_{12}	350.4	349.0	361.5	362.0	373.2	375.9
TE_{012}	357.4	356.3	368.6	370.9	365.7	366.6
TM_{011}	362.7	362.3	421.8	426.7	419.8	422.1

Table 3.1: Modes simulated and measured.
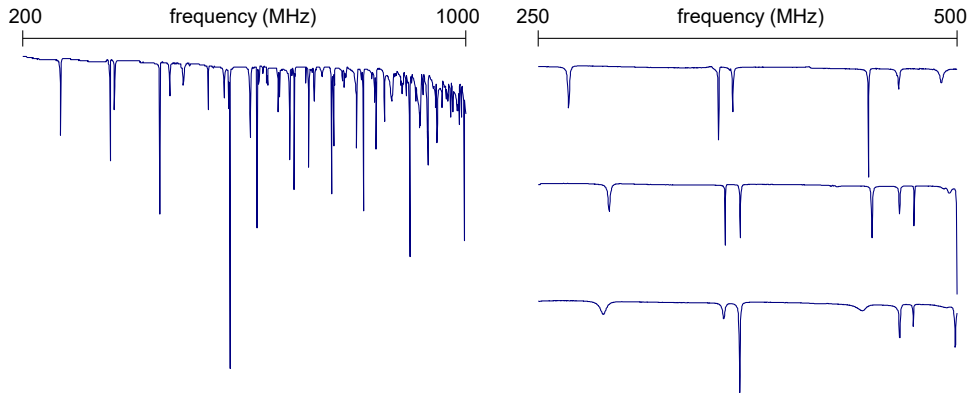
Figure 3.1: (Left) S_{11} plot from a small (1 cm diameter) unmatched pick-up loop placed to the side of the ceramic cylinder at its half-height. A large number of different modes can be detected. (Right) Expanded view of the 250–500 MHz range with the HEM_{11} mode at the lowest frequency: top – full cylinder; centre – cylinder with an empty 2.5 cm diameter hole drilled in the centre; bottom – a human finger is positioned inside the hole

Figure 3.2 shows simulated changes in the resonance frequency for different hole diameters in an unshielded HEM resonator, and for different shield diameters for an HEM resonator with a 2.5 cm diameter hole filled with tissue. Two inductively coupled impedance matching networks were placed at the centre of the long axis of the resonator at a distance of 1.2 cm from the outside surface of the resonator, 90° apart from each other: the topology of the coupling loops is shown in Figure 3.3. The variable capacitors allow fine-tuning for different loads. Figure 3.4 shows a photograph of the assembled HEM resonator. A PMMA cylinder (height 8 cm, inner diameter 14 cm, wall-thickness 9 mm) was used to form a closed annulus centring the ceramic cylinder while allowing access to the bore of the resonator. Inside the PMMA cylinder 25 μm thick copper foil (3M) was glued to form a shield. The coil was interfaced to the scanner by using 40 cm
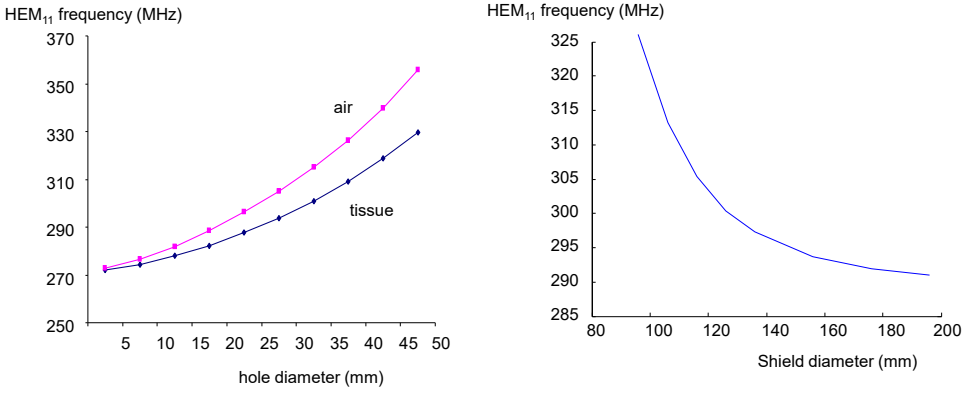
HEM$_{11}$ frequency (MHz)

HEM$_{11}$ frequency (MHz)

Figure 3.2: (Left) Plot of simulated HEM$_{11}$ frequency versus the diameter of the hole drilled through the centre of the resonator with the hole filled with either air or tissue. (Right) For a resonator with a 25 mm diameter hole filled with tissue, a plot of the HEM$_{11}$ frequency versus diameter of a thin copper shield with height equal to that of the resonator.
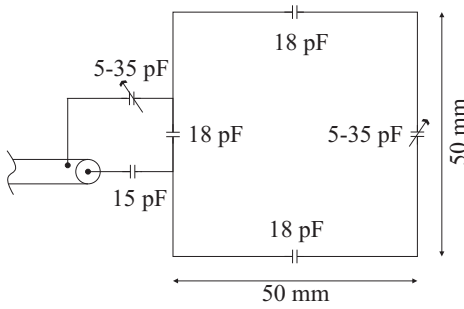

Figure 3.3: Topology of the coupling loop and matching network for the ceramic resonator.

long double-shielded 50 Ω coaxial cables (K 02252, Huber & Suhner, Switzerland). The resonator was matched to 298.1 MHz when loaded with a human finger and each channel achieved an S$_{11}$ of less than –20 dB. The S$_{21}$ between channels was also less than –20 dB. The effect of placing the finger inside the resonator is also shown in Figure 3.4. There is a significant reduction in the Q value of the resonator from 400 in the unloaded case to 150 when the resonator is loaded, with an ~3 MHz decrease in the resonance frequency.
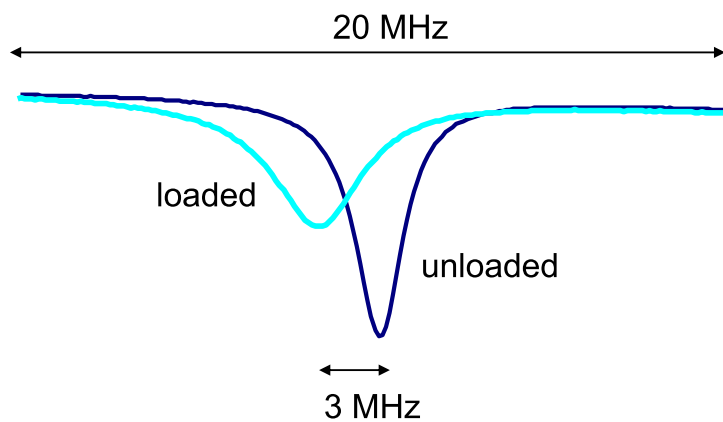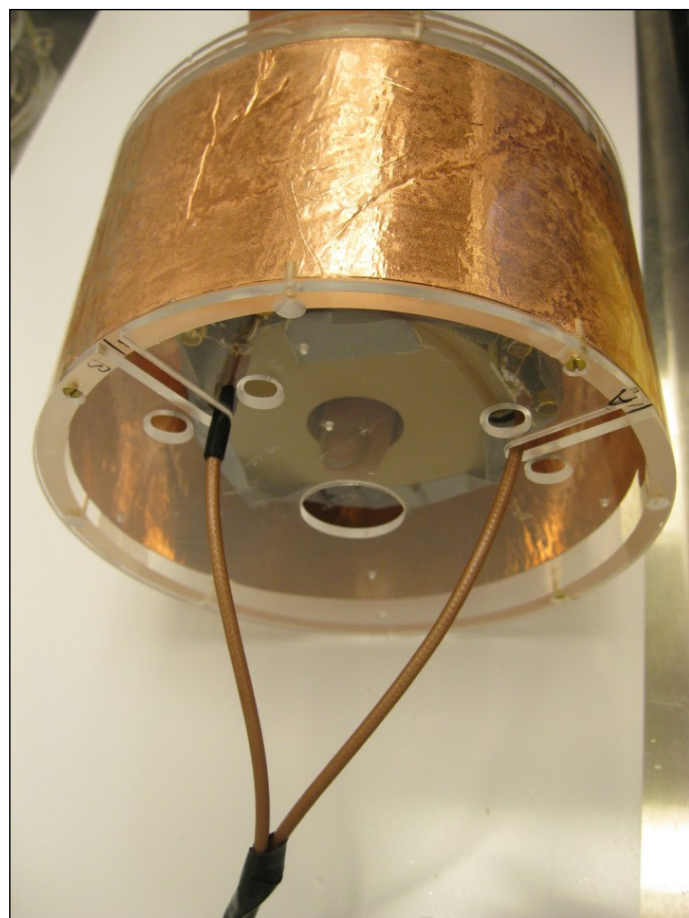
Figure 3.4: (Left) Photograph of the shielded quadrature HEM$_{11}$ resonator with coaxial cables feeding the two orthogonal matching networks. (Right) Effect of loading the resonator with a human finger.

3.3.2. PHANTOM MRI MEASUREMENTS

Experimentally acquired B_1^+ maps from the dielectric resonator are shown in Figure 3.5, depicting relatively homogeneous fields in both the transverse and longitudinal directions. As a measure of the transmit field efficiency, the B_1^+ field at the centre of the phantom was determined to be ~11.5 μT per $\sqrt{W}$ of power delivered to the coil. The acquired B_1^+ maps correspond well to the simulated data also shown in Figure 3.5. For the comparison loop-gap resonator, the B_1^+ field at the centre was measured to be ~8.2 μT/$\sqrt{W}$.
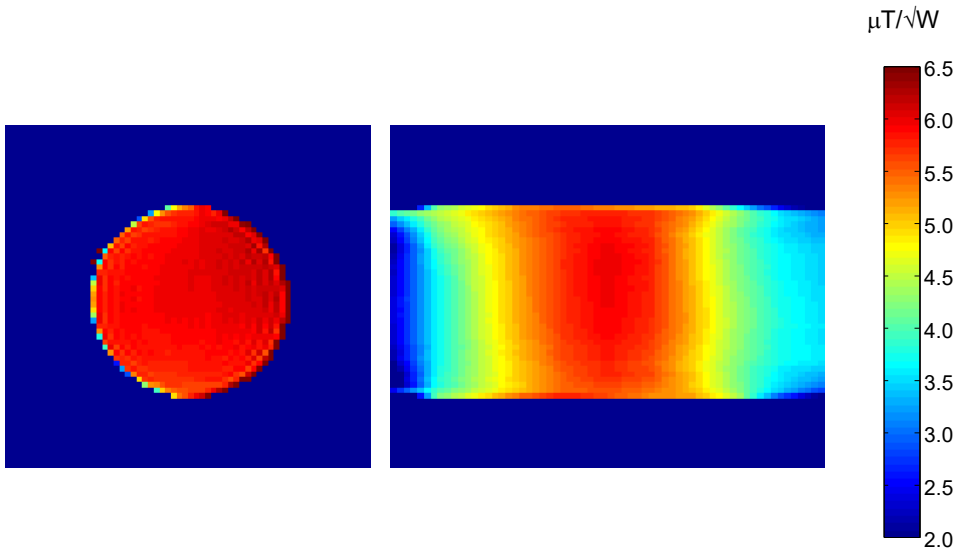

Figure 3.5: (Left) Transverse and coronal B_1^+ maps obtained using a saline phantom in the HEM resonator. (Right) Corresponding B_1^+ maps obtained using electromagnetic simulations. The axial extent of the B_1^+ field greater than 50% of its maximum at the centre is ~5 cm.

3.3.3. IN VIVO MRI EXPERIMENTS

Figure 3.6 shows results obtained from a healthy volunteer with the second digit of the right hand. The volunteer is positioned on the side with the hand placed slightly higher than the head, with the coil firmly held in place at the centre of the magnet. Insertion of every single digit is possible, with the remaining digits resting against the flat bottom of the coil. Best patient comfort occurs if the hand is supported with sandbags or other support materials. The aim is to study mainly the digital interphalangeal (DIP) and proximal interphalangeal (MIP) joints, so the finger does not have to be pushed into the coil to a full and uncomfortable extent. This situation can be favourably compared with conventional scans on 1.5 or 3 T systems in which the body coil is used for excitation, and the coil is placed over the entire wrist with the palm facing the upper part of the femur. The fingers are therefore in a sub-optimal position very close to the coil and gradients, and the specific absorption ratio (SAR)in this configuration is particularly high in body parts such as the arms and hands adjacent to the magnet bore. The images in Figure 6 are acquired at a spatial resolution of $0.15 \times 0.3 \times 0.5$ mm^3,significantly higher than at lower fields, and in a very short imaging time of ~1.5 min. The images show fine structure within the trabecular bone and the cartilage. Higher resolutions are of course possible with longer scanning times.
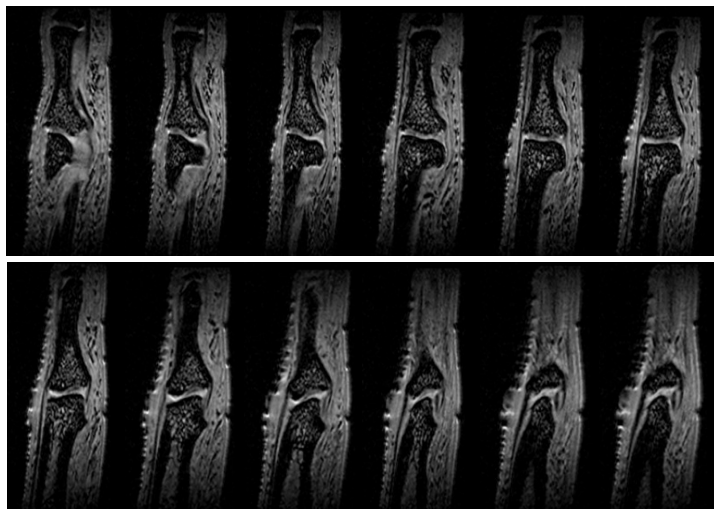

Figure 3.6: Images from a three-dimensional gradient echo sequence of the forefinger of the hand of a healthy volunteer. The spatial resolution is $0.15 \times 0.3 \times 0.5$ mm^3 and the images are acquired in ~1.5 min. The images show the fine resolution in the trabecular bone and cartilage structures.

3.4. Discussion

THIS paper has described the properties of a high-permittivity ceramic cylindrical resonator, and the design of an annular HEM_{11} resonator based upon this material. Electromagnetic simulations have been shown to correspond well to experimental measurements in terms of resonance frequencies, and the effects on these frequencies of a central hole and an outer RF shield. Therefore, resonators using different materials and with different geometries can be designed with a high degree of accuracy through simulations before the highly specialized process of ceramic production is initiated. The in vivo images acquired of the human finger show a high degree of RF homogeneity, and very high spatial resolution can be achieved in a relatively short imaging time.

One question is how large the hole diameter can be before the coil performance degrades severely. As the hole diameter increases, the B_1 field in the centre of the resonator becomes lower. Figure 3.7 shows plots of the magnetic field as a function of hole diameter, with the hole filled with tissue. The B_1 field can be seen to "spread out", but even for diameters which are about one-third of the diameter of the resonator itself the B_1 field maintains a reasonably homogeneous distribution. In the case of the 30 mm hole diameter, the B_1 field at the centre of the resonator is approximately 80% that of the resonator with no hole. Maintenance of the essential mode depends upon the electric field distribution not being disturbed significantly by the presence of a central hole. Since the electric field is zero at the centre for the HEM_{11} mode, increasing radially outwards, a hole diameter up to ~20 mm has minimal effect on the E-field distribution and strength, and therefore also on the magnetic field. However, when the hole "cuts into" volumes where the E-field is significant, then the mode becomes less effective, and the magnetic field much smaller, as is seen when the hole diameter increases to 30 mm.

In terms of building larger coils, what this implies is that one would move to a larger outer diameter for a given inner diameter, or use a material with a lower permittivity so that a larger resonator could be constructed. In this case the sample would have a more similar permittivity to the coil material, thus preserving essentially an undisturbed resonator. This can be seen in a previous paper on HEM mode resonators, in which water was the dielectric (with a permittivity very close to tissue) and the inner diameter of the hole can be made much larger [11].

One interesting aspect of these resonators is that the effects of shielding on the resonance frequency can potentially be used to create a double-tuned resonator for closely
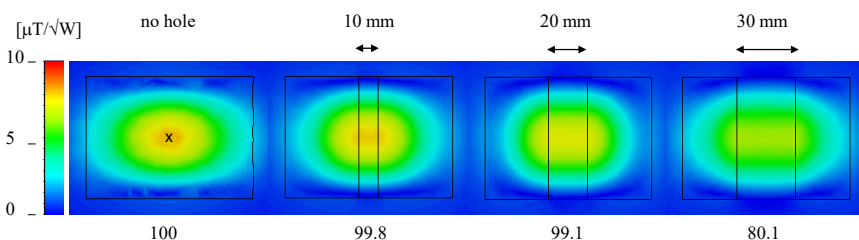
Figure 3.7: Electromagnetic simulations of the B_1^+ field in the HEM resonator as a function of hole diameter, with the hole filled with tissue. The numbers refer to the percentage of the B_1^+ field measured at the centre point (x) of the resonator with no hole present. When the hole diameter reaches 30 mm, the maximum B_1^+ field is no longer at the centre of the resonator, but at the edge of the inner hole, which explains the relatively large drop in value.

spaced frequencies such as fluorine (resonant frequency 280.4 MHz at 7 T) and protons, without the need for lumped element trap-circuits. Two possibilities are shown in Figure 3.8.
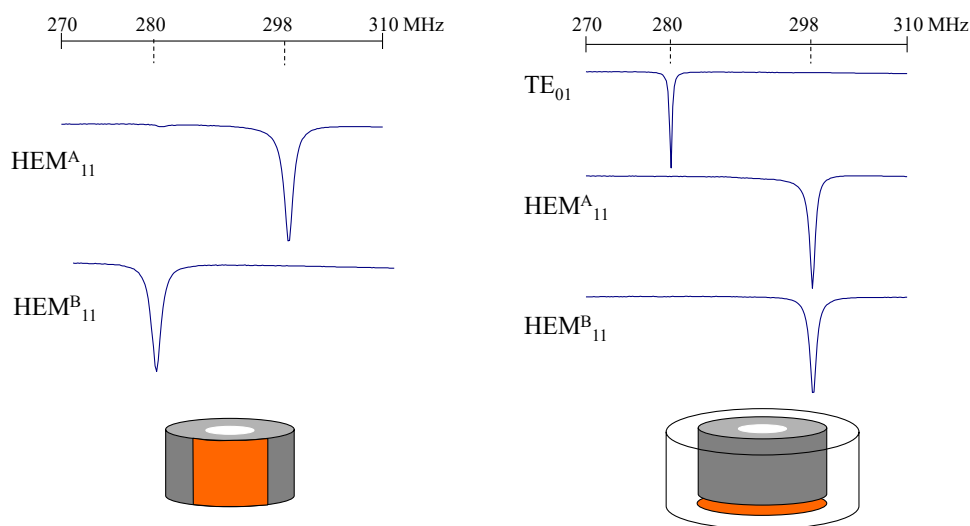

Figure 3.8: Two methods of double-tuning the ceramic resonator to proton (298 MHz) and fluorine (280 MHz) resonant frequencies at 7 T. On the left a partial (~90° coverage) shield shifts one of the HEM modes (denoted HEM^A) up to 298 MHz while the other mode (denoted HEM^B) is unaffected. On the right, an additional shield placed below the resonator shifts the TE mode from 251 MHz to 280 MHz while the two orthogonal HEM modes remain at 298 MHz.

On the left, a close shield, which subtends an angle of ~90°, shifts the frequency of one of the HEM modes upwards, but does not affect the orthogonal mode. The two network

analyser plots acquired with a pick-up loop oriented opposite the shield (detecting the mode denoted HEM[A]) and at 90° to the shield (detecting the mode denoted HEM[B]) show resonant frequencies at 298 and 280 MHz, respectively. Of course, one disadvantage of this approach is that only linear mode operation is possible for both frequencies. A second possibility, shown on the right in Figure 3.8, is to tune the TE_{01} mode to the fluorine frequency by using a shield on the bottom of the resonator, with the HEM modes largely unaffected by this shielding. Operation of this coil would involve rotation by 90° between using the quadrature HEM modes and the linear TE mode, but this design could be useful for imaging, for example, ex vivo tissue in which coil reorientation between scans is not a problem. Alternatively, one of the proton HEM modes could be used with the proton TE mode without the need for coil reorientation.

3.5. CONCLUSION

THIS work shows that high-permittivity material resonators are feasible for high-field MRI. Due to the material properties it is possible to build compact resonators with good B_1 field homogeneity. Design equations given in the literature allow construction of annular resonators with the aid of electromagnetic simulation software. The possibility to fine-tune the resonators with copper shields also eases the demands on very accurate manufacturing of the resonators. These resonators can also be used for smaller animal MR scanners, where even higher operational frequencies would allow still more compact designs.

REFERENCES

[1] S. Aussenhofer and A. Webb, *High-permittivity solid ceramic resonators for high-field human mri,* NMR in Biomedicine **26**, 1555 (2013).

[2] G. Annino, M. Cassettari, I. Longo, M. Martinelli, P. Van Bentum, and E. Van der Horst, *A novel probe head for high-field, high-frequency electron paramagnetic resonance,* Review of scientific instruments **70**, 1787 (1999).

[3] G. Annino, M. Cassettari, M. Martinelli, and P. Van Bentum, *A nonradiative approach to single-mode dielectric resonators,* Applied Magnetic Resonance **24**, 157 (2003).

[4] K. Haines, T. Neuberger, M. Lanagan, E. Semouchkina, and A. Webb, *High q calcium titanate cylindrical dielectric resonators for magnetic resonance microimaging,* Journal of Magnetic Resonance **200**, 349 (2009).

[5] T. Neuberger, V. Tyagi, E. Semouchkina, M. Lanagan, A. Baker, K. Haines, and A. Webb, *Design of a ceramic dielectric resonator for nmr microimaging at 14.1 tesla,* Concepts in Magnetic Resonance Part B: Magnetic Resonance Engineering **33**, 109 (2008).

[6] P. Daleiden, M.-A. Golombeck, S. Junge, and O. Dössel, *Development and characterisation of a ceramic hf-resonator for the mr-tomography,* Biomedizinische Technik/Biomedical Engineering **47**, 758 (2002).

[7] E. Eriksen, M.-A. Golombeck, S. Junge, and O. Dössel, *Simulation of a birdcage and a ceramic cavity hf-resonator for high magnetic fields in magnetic resonance imaging,* Biomedizinische Technik/Biomedical Engineering **47**, 754 (2002).

[8] S. M. Mattar and S. Y. ElNaggar, *Analysis of two stacked cylindrical dielectric resonators in a te 102 microwave cavity for magnetic resonance spectroscopy,* Journal of Magnetic Resonance **209**, 174 (2011).

[9] A. Neufeld, N. Landsberg, and A. Boag, *Dielectric inserts for sensitivity and rf magnetic field enhancement in nmr volume coils,* Journal of Magnetic Resonance **200**, 49 (2009).

[10] H. Wen, F. A. Jaffer, T. J. Denison, S. Duewell, A. S. Chesnick, and R. S. Balaban, *The evaluation of dielectric resonators containing h 2 o or d 2 o as rf coils for high-field mr imaging and spectroscopy,* Journal of Magnetic Resonance, Series B **110**, 117 (1996).

[11] S. A. Aussenhofer and A. G. Webb, *Design and evaluation of a detunable water-based quadrature hem11 mode dielectric resonator as a new type of volume coil for high field mri,* Magnetic Resonance in Medicine **68**, 1325 (2012).

[12] A. Kishk, A. Glisson, and G. Junker, *Bandwidth enhancement for split cylindrical dielectric resonator antennas,* Progress In Electromagnetics Research **33**, 97 (2001).

[13] D. Kajfez, A. W. Glisson, and J. James, *Computed modal field distributions for isolated dielectric resonators,* IEEE transactions on Microwave Theory and Techniques **32**, 1609 (1984).

[14] V. L. Yarnykh, *Actual flip-angle imaging in the pulsed steady state: a method for rapid three-dimensional mapping of the transmitted radiofrequency field,* Magnetic resonance in Medicine **57**, 192 (2007).

[15] W. Froncisz and J. S. Hyde, *The loop-gap resonator: a new microwave lumped circuit esr sample structure,* Journal of Magnetic Resonance (1969) **47**, 515 (1982).

[16] A. Webb, *Visualization and characterization of pure and coupled modes in water-based dielectric resonators on a human 7t scanner,* Journal of Magnetic Resonance **216**, 107 (2012).

[17] M. Jaworski and M. W. Pospieszalski, *An accurate solution of the cylindrical dielectric resonator problem,* Microwave Theory and Techniques, IEEE Transactions on **27**, 639 (1979).

[18] F. S and A. JELENSKI, *Influence of conducting walls on resonant frequencies of dielectric microwave resonator,* (1971).

3